Thermal and vibrational characterization of human skin

Rong Tang, Valérie Samouillan, Jany Dandurand, Colette Lacabanne, Florence Nadal-Wollbold, Christiane Casas, Anne-Marie Schmitt

DOI 10.1007/s10973-016-5384-z

Thermal and vibrational characterization of human skin

Influence of the freezing process

Rong Tang[1] · Valerie Samouillan[1] · Jany Dandurand[1] · Colette Lacabanne[1] · Florence Nadal-Wollbold[2] · Christiane Casas[2] · Anne-Marie Schmitt[2]

Abstract For a better understanding of the molecular and organizational changes in human dermis, biophysical methods were tested. The aim of this study was to find suitable and reproducible biomarkers for further clinical studies on intrinsic and extrinsic aging of dermis. Thermoporometry, hydric organization and thermal transitions of fresh and frozen skins were determined by differential scanning calorimetry (DSC). Fourier transform infrared spectroscopy (FTIR) was used to identify the absorption bands of the dermis especially in the 1800–1000 cm^{-1} zone and to discriminate between the different secondary structures of proteins. A widening of the pore size distribution is evidenced with freezing, but there is no significant difference between the hydric organization and the endothermic collagen denaturation of fresh and frozen skins. The global FTIR spectra and the second derivative spectra in the scanned zone are also identical in fresh and frozen dermis, validating the storage protocol. DSC and FTIR are well-suited techniques to characterize human skin, giving accurate results with high reproducibility. The acquisition of thermal and vibrational biomarkers of the skin at the mesoscale and nanoscale contributes to its better knowledge and is promising for further studies on skin aging.

✉ Valerie Samouillan
valerie.samouillan@univ-tlse3.fr

[1] CIRIMAT UMR 5085, Institut Carnot, Equipe Physique des Polymères, University of Toulouse, 118 route de Narbonne, 31062 Toulouse Cedex, France

[2] Pierre Fabre Dermo-Cosmetique, Skin Research Center, Hôtel-Dieu saint Jacques, 31025 Toulouse Cedex 3, France

Keywords Collagen denaturation · DSC · Fourier transform infrared spectroscopy · Human skin · Hydration · Secondary structures of proteins

Introduction

With a growing elderly population, interest in general skin health and skin homeostasis has been increasing. Understanding hydration in skin is of primary importance to the medical and cosmetic communities. In particular, the ability to differentiate protein bound from bulk water is of interest in studies ranging from the evaluation of therapeutics for wound healing to the hydration efficacy of skin care products. Skin is the largest body organ and is easily accessible. A great number of clinical studies have been performed on skin biopsies to help the understanding on mechanisms involved in intrinsic and extrinsic (photo-) aging [1, 2] using histological and ultrastructural approaches. Unfortunately, the complexity and slowness of the aging processes leading to subtle changes of biological function (including biochemical, morphological, physical aspects) provide the aging research with enormous difficulties.

The skin consists of the epidermis and dermis, and the latter is thought to be more important in determining the physical properties of skin. Among the various components of the dermis, extracellular matrix consisting of collagens, elastic fibers and amorphous ground substances is strongly involved in the process of cutaneous aging [3], in close correlation with changes in hydration [4, 5]. Collagen, the most abundant component in the dermis, comprises 80 % of the tissue total dry mass and 90 % of all dermal proteins. If at least half of the twenty eight types of collagens are present in skin, the fibril-forming collagens I, III and V are

the most abundant. Collagens I and III represent close to 90 and 10 %, respectively, in the composition of dermal collagen fibrils, and collagen V is present as a minor fraction of about 2 %. Altogether, the fibrils with their associated proteins confer tensile strength to the skin and are pivotal for the general organization and stability of the dermal extracellular matrix among other functions [6]. The dermis can also be divided into two layers: the papillary dermis and the reticular dermis. The papillary dermis layer contains much thinner and less packed of collagen type III fibers, and it is more fibroblastic than the reticular dermis layer [7]. It is also shown that the papillary dermis contains much more components of glycosaminoglycans such as hyaluronic acid and dermatan sulfate [8]. In the dermis, collagen bundles form a three-dimensional mesh with other fibrillar proteins and interstitial cells, including a network of contractile fibroblasts. The structure is cemented by a hyaluronic acid and proteoglycan gel that allows for viscous flux and mediates interchange of water nutrients and metabolites between the blood, the lymph, the interstitial cell network and the epidermal layers [9]. The recent studies propose a refined skin-associated adipocytes as dermal adipose tissue, historically termed subcutaneous adipose, hypodermis and subcutis, which underlie the reticular dermis. The major hygroscopic agents, glycerol and hyaluronic acid play a key role in sky hydration and consequently prevent skin aging [10]. Furthermore, the cutaneous aging could be accelerated by the decrease of overall collagen types after menopause [11].

New information on whole skin and dermis can be reached at the molecular level trough near-infrared diffusive reflection (NIR-DR) [12, 13], Fourier transform infrared spectroscopy/attenuated total reflectance (FTIR/ATR) [12, 14, 15], Raman spectroscopy [16–19], nuclear magnetic resonance/magnetic resonance imaging (NMR/MRI) [15, 20, 21], dynamic vapor sorption (DVS) [19], changes in collagen hydration with age yield somewhat conflicting results, which could be attributed to the preparation of samples.

Combined with thermogravimetric analysis (TG) measurements, differential scanning calorimetry (DSC) is a standard method to evaluate freezable and unfreezable water [22–25]. DSC is also an appropriate method for assessing protein thermal stability and conformational changes. It is peculiarly well suited to evaluate the thermal stability of purified collagens in solution or in their aggregated form [26], or directly in native tissues [26–34] and biomaterials [28–30]. It has been successfully applied to characterize collagen both in animal and human skins [35–37]; nevertheless, few DSC data are available on human dermis, despite the ability of this technique to evidence evolution of the major proteins of dermis under physical or pathological factors, such as collagen alteration in irradiated human dermis [37], increased collagen stability with glycation induced by diabetes [38] or modification of collagen I/III in scars and keloids [39].

If punch biopsies from living patients are routinely taken for histologic assessment in vitro, few biophysical studies have been performed on such samples. The first objective of this work is to evaluate the effect of a quenching/storage protocol on fresh human skin explants for the scheduled clinical study on a large panel of young and aged patients. Simultaneously, it is essential to validate the combined use of DSC and FTIR techniques to obtain reproducible data from these small biopsies removed from living patients and to establish a routine protocol to analyze an important number of samples. The final aim of this work was to extract suitable biomarkers of the hydric organization and biomacromolecules integrity from the thermal and vibrational fingerprints of safe skin.

Materials and Methods

Materials

Fresh human abdominal skin disks (22 mm by diameter) were collected by BIOPREDIC Society (BIOPREDIC INTERNATIONAL, SAINT GREGOIRE, FRANCE) from 5 female patients (Caucasian type, 25–50 years old) undergoing abdominoplasty. The skin samples were first rinsed with PBS. Then, the adipose tissue/hypodermis was removed. The handling of the fresh skin was done under hood (natural atmosphere) to minimize contamination. Fresh portions were stored at 4 °C for 24 h, and explants (4 mm by diameter, 5–7 mg by mass) were removed from these portions using a biopsy punch. Twenty explants could be extracted for a skin disk. A series of explants (*fresh explants*) were immediately analyzed. Another series of explants (*stored explants*) were stored in Eppendorf tubes and then quenched in liquid nitrogen for several minutes and stored at −20 °C for 8 days. Before further analyses, these frozen samples were thawed at 4 °C for 1 h.

Differential scanning calorimetry (DSC)

DSC measurements were performed with a DSC Pyris calorimeter (PERKIN ELMER, Waltham, MA) using an empty pan as reference. The calorimeter was calibrated using the manufacturer's instructions with pure water, cyclohexane and indium as standards, resulting in a temperature accuracy of ±0.1 °C and an enthalpy accuracy of $\pm 2.10^{-4}$ J kg^{-1}. Temperature calibration was undertaken at each scanning rate. Fresh and frozen explants (5–7 mg by mass) were sealed in hermetic aluminum pan. Samples were cooled at 10 °C min^{-1} to −30 °C (1st cooling scan),

then held 10 min to freeze water. For thermoporometry measurements (TPM), scans were conducted from −30 to 20 °C at a low scanning rate, 0.5 °C min^{-1}, to avoid thermal and time delays in the DSC curve.

To determine freezable water amount and intrinsic thermal transitions, the samples were heated at 10 °C min^{-1} to 85 °C (1st heating scan), then cooled at −10 °C min^{-1} to −30 °C (2nd cooling scan) and then heated at 10 °C min^{-1} to 85 °C (2nd heating scan).

After completing the DSC measurements, pans were reweighted to check that they had been correctly sealed. The sample pans were pierced and dried to constant mass at 195 °C for 10 min to determine the sample dry mass and the total water mass.

Fourier transform infrared analysis (FTIR)

Fourier transform infrared spectroscopy/attenuated total reflectance (FTIR/ATR) spectra were acquired using a Nicolet 5700 FTIR (THERMO FISHER SCIENTIFIC, Waltham, MA) equipped in ATR device with a KBr beam splitter and a MCT/B detector. Explants (dermis face) were directly laid on the ATR accessory (Smart Orbit with a type IIA diamond crystal, refractive index 2.4) and covered by a hermetic cap with an 'O' ring to avoid dehydration of the sample during spectra acquisition. Spectra were recorded over the region of 4000–450 cm^{-1} with a spectral resolution of 2 cm^{-1} and 80 accumulations. Spectral data were collected using Omnic 8.0 (THERMO FISHER SCIENTIFIC, Waltham, MA). A single-beam background spectrum was collected from the clean diamond crystal before each experiment and this background was subtracted from the spectra. Spectra were then subjected to ATR and baseline corrections and normalized in the amide II region. For each type of explant, a mean representative spectrum and its second derivative were computed. Second derivatives and Fourier self-deconvolution (FSD) were used to enhance the chemical information present in overlapping infrared absorption bands. Second derivatives were also used to circumvent baseline drifts in infrared spectra.

Statistical analysis

All experiments were performed with at least three replicates for each group and for at least three independent repeats. Quantitative values are shown as mean ± SEM. In statistics, we practiced one-way analysis of variance (one-way ANOVA) to compare the means of the samples. The p-value was also used to determine the significant difference between groups. It was considered statistically significant threshold of p-value less than 0.05.

Results and discussion

Thermal characterization

Thermoporometry measurements (TPM)

DSC curves of fresh and stored explants are plotted in Fig. 1. In both curves, two distinct endothermic peaks were recorded in the zone of ice melting, what is an evidence for the existence of pores filled by water in the explants. It is well known that structure and connectivity of pores in skin influence the heat and mass transport processes associated with the thermoregulatory function of the organ [40]. As commonly observed in mesoporous hydrophilic materials, the low temperature peaks are assigned to the melting of the ice confined in the pores while the second ones result from the melting of the ice outside the pores (excess water) [41–44].

According to the Gibbs–Thomson effect, Brun et al. [41] established that the radius r_p of hypothetical cylindrical pores filled by water and the differential pore volume dV/dr_p could be calculated from the melting point depression ΔT and heat flow dQ/dt. The following equations are as follows:

$$r_p(\text{nm}) = \frac{-32.33}{T} + 0.68 \quad \text{with } \Delta T = T - T_0 \text{ and } -40 < \Delta T < 0 \tag{1}$$

$$\frac{dV_p}{dr_p} = \frac{dQ}{dt} \times \frac{dt}{d(\Delta T)} \times \frac{d(\Delta T)}{dr_p} \times \frac{1}{m\Delta H_f(T)\rho(T)} \tag{2}$$

where $d(\Delta T)/dt$ is the scanning rate of the DSC experiments, m is the mass of dry material, and ΔH_f and ρ the heat of fusion and density of water, respectively. The

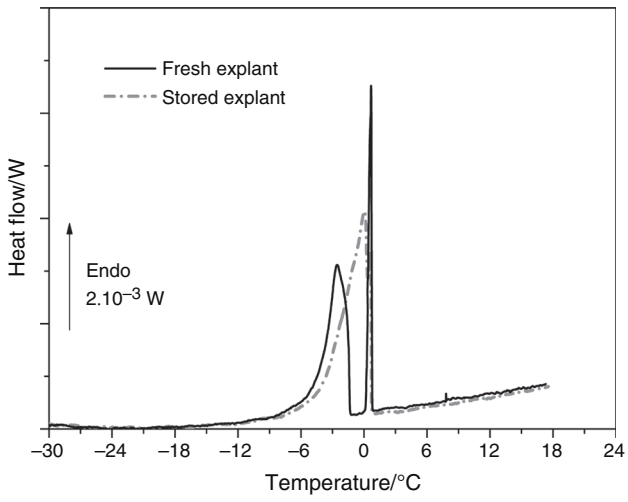

Fig. 1 Representative DSC curves for a matched set of fresh and stored skin explants (scanning rate 0.5 °C min^{-1})

following values were used: $\Delta H_f(T) = (334.1 + 2.119T - 0.00783T^2) \times 10^{-3}$ (J kg^{-1}) and $\rho(T) = 917 (1.032 - 1.17 \times 10^{-7}T)$ (kg m^{-3}) [45].

For the present study, pore radius was calculated on the assumption of cylindrical pore shape. This is unlikely to be absolutely correct, but is believed to be a reasonable approximation for the elongated voids expected within skin, and it has been successfully used for fibrous materials [40, 46, 47]. Using Eq. (1), the temperature axis of TPM measurements can be converted into a pore size scale; in this study, T_0 was determined experimentally as the onset temperature of the second endothermic peak. After a baseline subtraction step that effectively removes the underlying heat capacity contribution to the DSC signal, the heat flow curve, dQ/dt, was converted into a differential pore volume using Eq. (2). The resulting pore size distributions (PSD) determined for fresh and stored explants are reported in Fig. 2. From Fig. 2, we can note a relatively narrow size distribution for the fresh skin; since the radius of pores range from 0 to 20 nm, these pores can be classified as mesopores. The storage protocol (quenching and storage at −20 °C during 8 days) leads to a widening of the pore size distribution, in peculiar enhancing the formation of macropores with radius from 20 to 60 nm.

Even if the scans at 0.5 °C min^{-1} can be used to quantify total freezable water, the main objective of this study was to establish a robust protocol to determine with a single DSC scan, preferentially low time-consuming, both the hydration and the intrinsic transitions of dermal proteins. Comparison of DSC curves performed at different scanning rates between 0.5 and 20 °C min^{-1} (not shown here), evidenced that a scanning rate of 10 °C min^{-1} was the optimal choice to reduce the experimental time and to measure reproducible and well-defined ice melting and protein denaturation in skin biopsies.

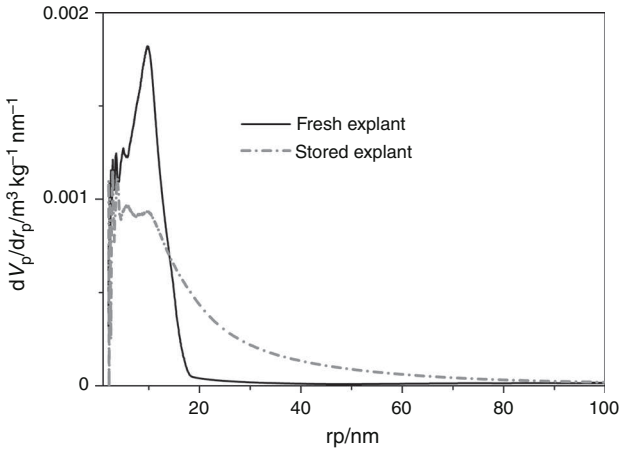

Fig. 2 Representative differential pore size distributions from TPM measurements for a matched set of fresh and stored skin explants

Water quantification and collagen denaturation

In Fig. 3 are reported the DSC curves (normalized to the initial mass) of fresh and stored explants corresponding to the first cooling between 20 and −30 °C and the successive heating at 10 °C min^{-1} between −30 and 30 °C; for the sake of clarity, only one curve for each type of sample is reported and an enlargement is made in the temperature zone of ice crystallization/melting. The discussion has focused on melting peaks only, because the ice crystallization temperature is usually not reproducible for a super cooled liquid [42]. As already observed in TPM measurements at 0.5 °C min^{-1}, the endothermic peaks recorded in this temperature zone correspond to the melting of freezable water, even if in this case the resolution into separated peaks is not achieved because of the scanning rate. This extrinsic transition is widely used to quantify the amount of total freezable water in hydrated proteins and tissues (by dividing the area of the measured endothermic peak by 0.334 J kg^{-1}, corresponding to the melting enthalpy of pure ice at 0 °C) [23, 48], and completes thermogravimetric analyses giving the total amount of water. The amount of unfreezable water can be calculated by a simple difference. This quantification was performed for all the samples and reported in Fig. 4.

The total hydration of fresh skin is 66.2 ± 1 %, distributed in 41.7 ± 0.5 % of freezable water and 24.5 ± 1.1 % of unfreezable water. It must be pointed out that the determination of freezable water from the area of the endotherms recorded at 0.0083 °C s^{-1} leads to similar values.

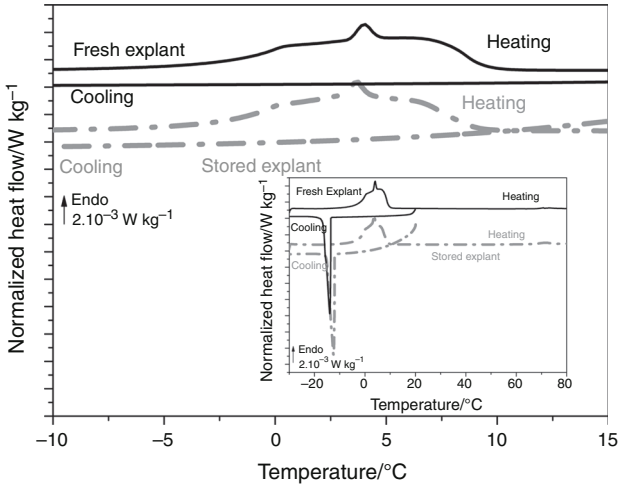

Fig. 3 Representative DSC curves for a matched set of fresh and stored skin explants [cooling and successive heating, scanning rate 10 °C min^{-1} and enlargement in the (−30; 30 °C) window]. Whole curves in the *inset*

The total hydration of fresh skin is consistent with literature data, [10, 36], giving an average value of 65–70 % for the hydration of human dermis and epidermis; this remarkably high value, corresponding to about 2 kg of water per kg of dry matter, is due to a combination of physical and chemical factors including the presence of interconnected pores, the peculiar hygroscopic nature of hyaluronic acid and the hydrophilicity of collagen. If a well-documented literature is present for the total hydration of stratum corneum, epidermis and dermis measurable by different biophysical techniques [5], few data, obtained from Raman spectroscopy [19, 49], DVS [19] and NMR [21] are reported on the quantification of the different kinds of water (namely free and bound waters) in human skin. The present DSC study shows that the freezable water roughly represents two-third of the total water in human skin. The term freezable water is preferred to the term 'free' water—rather reserved to vibrational or relaxational techniques—since it covers bulk water in excess but also confined water in mesopores, as previously shown by TPM. In accordance with previous NMR, DVS and Raman results [19, 21], this work evidences that bulk water is present in relatively large quantity in safe human skin. One-third of the total water of human skin is unfreezable water. To avoid confusion, in this study, the term 'unfreezable water' is preferred to the term 'bound' water, which refers to water directly bound to protein via hydrogen bonds in the first hydration shell, but that can also be extended to the multilayer hydration shell and identified as a slowing down of the dynamics in dielectric and NMR techniques [24, 50–54]. Besides the idea of monolayer, multilayer and free water as defined for S-shaped sorption isotherms, the types of water can be also divided by their behavior during freezing and thawing, and in this case bound water is sometimes divided in 'unfreezable bound water'—strongly associated with hydrophilic groups—and 'freezable bound water'—less closely bound and immobilized in DSC experiments [55, 56]. In our case, unfreezable water is 'unfreezable bound water' and it corresponds to the filling of the first hydration shell of proteins and other hydrophilic components such as HA; the value of 24.5 % of unfreezable water, corresponding to 0.72 kg of unfreezable water per kg of dry matter, is consistent with literature data on biological tissues [22, 57]. Usually, about 0.3–0.7 kg of unfreezable water remains associated per kilogram of a 'dry' protein [58]. Assuming that the average molar mass of one amino acid in collagen is 0.1 kg mol^{-1}, a roughly approximation leads to a value of 4 mol of water per moles of amino acid of collagen, which is slightly higher than the value determined by DVS [59] or X-ray diffraction for adsorbed multilayer water in collagen and collagen peptides [60], certainly because of the presence of HA in dermis.

The statistical analysis do not indicate any significant difference between the amounts of total, freezable and unfreezable waters in fresh and stored skins, evidencing that the quenching/storage protocol of the skin explants, even if it induces a widening of size pore distribution, does not induce quantitative modifications of the global hydric organization of the samples. The first hydration shell of the proteins is well conserved during the storage procedure.

In Fig. 5, the DSC curves of fresh and frozen skins recorded at 10 °C min^{-1} between −30 and 85 °C in the 60–85 °C zone are reported. Superimposed on this figure is the DSC curve of a decellularized bovine pericardium in the native state, which is a relatively simple and uniform tissue mainly constituted by type I collagen and representative of the thermal answer of hydrated collagen.

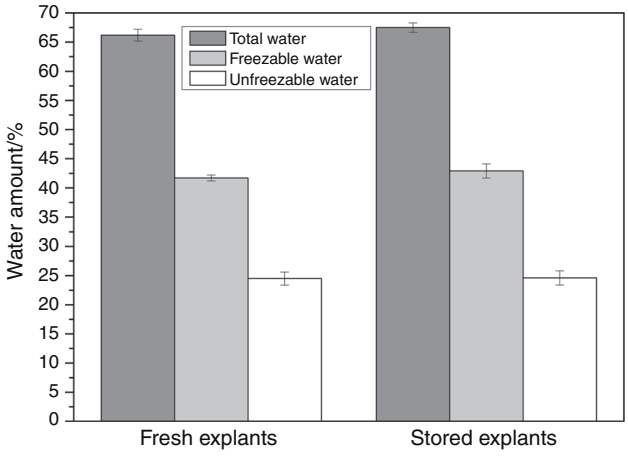

Fig. 4 Hydric organization of fresh and stored skin explants

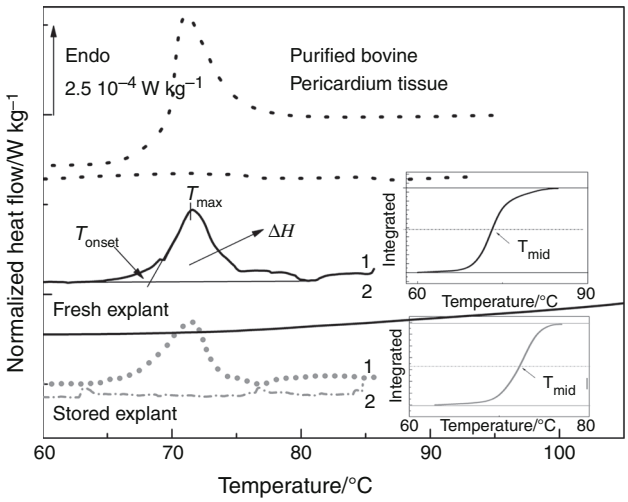

Fig. 5 Representative DSC curves for a matched set of fresh and stored skin explants and pericardium tissue [first and second heating, scanning rate 10 °C min^{-1} and enlargement in the (60–85 °C) window]

In a similar way as in bovine pericardium, in skin biopsies an endothermic phenomenon is recorded in this temperature zone during the first heating and associated with the irreversible thermal denaturation of collagen (not observed on successive scans). Small reversible endothermic events can be sometimes detected on the first and second scan and attributed to the reversible phase transitions of lipids [61, 62]. Nevertheless, when the hypodermis is correctly removed, these peaks can be neglected and do not interfere with the collagen answer.

In Fig. 5, the main characteristics of the denaturation peak T_{onset}, T_{max} and T_{mid} and the area under the endotherm peak are shown. T_{mid} represents the temperature at which 50 % of collagen is denatured. Whole integral area of the heat flow is reported in the inset of Fig. 5, allowing the determination of T_{mid} at the temperature midpoint. T_{onset}, T_{max} and T_{mid} are alternatively taken as the denaturation temperature according to the previous studies [34, 37, 39, 63, 64] while ΔH once normalized to the dry mass gives a measure of the specific heat/enthalpy of denaturation. It is well known that the characteristic feature of type I and type III collagens is the triple helical structure of three left-handed polyproline type helices twisted into a right-handed super helix. The formation of such a structure is due to the repeating sequence Gly-XY, where X and Y are often proline and hydroxyproline, respectively, and hydrogen bonding takes place between chains within the triple helix. On heating, the triple helix unfolds to produce random chains of gelatin that can remain covalently linked to each other or not depending on the degree of heating [65, 66]. The collagen denaturation—distinct from degradation—is a thermally activated process that involves rupture of hydrogen bonds coupling the three α-chains and a rearrangement of the triple helix into a random chain configuration [26]. If collagen denaturation was firstly described like a 'polymer melting' [67], detailed calorimetric studies are clearly consistent with the 'polymer in a box' mechanism, in which the molecule is thermally stabilized by confinement [27].

Differences in thermodynamic parameters of denaturation for proteins are believed to reflect the differences in their native states [68]. The denaturation temperature and the associated denaturation enthalpy are sensitive to the level of hydration, cross-links within and between molecules and to the amount and character of side chains exposed to the surrounding medium during unfolding [32]. Lowering of the expected denaturation temperature can indicate collagen degradation, fragmentation or expansion of the collagen lattice structure [33, 36, 37], while an increase of this temperature can be due to the formation of heat-stable cross-links, as observed in aged skins [34] or in chemically cross-linked collagenous biomaterials [28]. A change in enthalpy can indicate molecular degradation, denaturation or modification of the heat-labile bonding in the collagen molecules [33, 36, 37]. Since collagen denaturation in skin was shown to be multi-component [34–36], it can be interesting to calculate the mean reciprocal temperature $(1/T)_{mean}$, averaged over the whole endotherm and more representative of the thermal stability of collagen as proposed by Miles et al. [36].

$$\frac{\bar{1}}{T} = \int_{T_i}^{T_f} \frac{1}{T} \frac{C_p}{\Delta H} dT \tag{3}$$

where T_i and T_f are the lower and upper temperature limits of the endotherms.

The different thermal parameters of collagen denaturation in skin explants are reported in Fig. 6 for fresh and stored samples. For a better comparison, the reciprocal of $(1/T)_{mean}$ was converted into °C and displayed in the same figure. It must be pointed out that T_{max} and the reciprocal of $(1/T)_{mean}$ are displayed with a very small standard error for the studied samples, what validates the use of DSC to quantify the denaturation phenomenon.

In the case of fresh skins, the T_{max} temperature, which is generally ascribed to the denaturation temperature is 71.6 ± 0.5 °C; it is in the same line of order than the thermal parameters of hydrated rich collagenic tissues reported in literature and measured with the same scanning rate such as rat tail tendon [27], pericardium tissue [57] and skins from animals [36]. It was previously shown that the denaturation temperature drastically increases as the hydration decreases [27, 57], due to the decrease of intrafibrillar water content compacting the packing of fibers, and to the replacement of protein–protein hydrogen bonds by protein–water hydrogen bonds. This denaturation temperature is independent on hydration for tissues hydrated above 1 kg of water per kg of dry tissue [37] or 30 mol of water per three residues [27] (which corresponds to 1.8 kg of water per kg of dry matter). It is must be

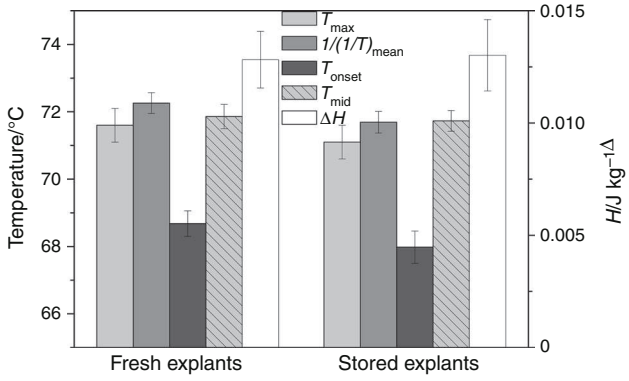

Fig. 6 Main thermal characteristics of the denaturation endotherm in skin samples

pointed out that this condition is checked for the studied samples, with a total hydration of 2 kg per kg of dry matter. In this case, the temperature range of the denaturation phenomenon can be considered as an intrinsic characteristic of collagens in the skin.

T_{mid} and T_{onset} have also been computed for this study, and in this case also there is no significant difference between the temperature values from fresh and stored explants; T_{onset} is of course located in a lower zone than T_{max}, and error bars of T_{onset} are a little wider than T_{mid}. T_{mid} is in the same temperature range as T_{max} and the reciprocal of $(1/T)_{mean}$.

The reciprocal of $(1/T)_{mean}$, which is assumed to be equal to T_{max} for narrow and symmetric endotherm peak, is in this case slightly upper than T_{max}, highlighting the asymmetry of the endotherm in skin samples, as already observed on other collagenic tissues [36]. The standard error is very weak for this parameter. Since it takes into account the proportion of the heat-stable cross-links in the denaturation phenomenon (in contrast with T_{max}, T_{onset} and T_{mid}), it can be considered as the preferential biomarker of the thermal stability of collagens in skin for further studies.

The denaturation enthalpy of human fresh skin is evaluated at 0.0128 J kg^{-1} of dry matter, with a standard error of about 10 %. This value that can be considered rather low when compared to pure collagenic tissues such as tendon or animal skins (ΔH comprised between 0.03 and 0.06 J kg^{-1}); first it must be reminded that some analyses are normalized to the real content of collagen (and not to the dry tissue). Moreover, in the present samples, neither epidermis nor cellular components were removed, decreasing the amount of collagen in the samples. Only few data are available on the denaturation enthalpy of fresh human skins [35, 39], and our values perfectly fit with Wiegand et al. ones, with a denaturation enthalpy of 0.0045 J kg^{-1} of fresh tissues for intact female skin (which corresponds to 0.013 J kg^{-1} of dry tissue). Moreover, it was shown that in a similar way as the denaturation temperature, the denaturation enthalpy was widely affected by hydration. At very low hydration, the enthalpy is one-fifth of the enthalpy of the fully hydrated triple helix, which implies that, compared with the fully hydrated state, the triple helix at very low hydrations is held together by one-fifth of its original number of hydrogen bonds. It reaches a constant value above 30 mol of water per three residues [27], and this condition of hydration is checked for the present skin samples. So ΔH can be used as a suitable biomarker for the hydrogen bonds network of hydrated collagen in skin.

No significant difference at the 0.05 level were found between the mean values of T_{max}, $1/(1/T)_{mean}$ and ΔH of fresh and stored explants, evidencing that the storage protocol do not impair the thermal stability of collagens in human skin: The hydrogen bonds network, the packing of the fibers and the triple helical domain are completely conserved with a quenching at −196 °C and a consecutive storage at −20 °C.

Vibrational characterization

FTIR technique in the transmission mode was first devoted to the analysis of lyophilized biological tissues because of the main absorption of water hiding all the other vibration modes; in the ATR mode, native biological tissues can be directly set on the crystal without any other preparation and kept at a constant hydration. This technique is widely applied to investigate in vivo or in vitro the outermost layer of human skin, i.e., the stratum corneum [61, 62, 69–73], but few data are available on the internal layer of human skin, i.e., reticular dermis. The penetration depth of the evanescent wave can be estimated with the refraction index of the crystal and the tissue, the frequency and incident angle of the radiation [73]. The measuring depth of ATR-FTIR in the skin is typically a few microns over the wave number window 4000–650 cm^{-1} [74].

In Fig. 7, the mean representative FTIR spectra of fresh and stored explants (corresponding to the reticular dermis) in the 2000–950 cm^{-1} zone are reported; to assist the assignment of the different vibration bands of dermis, the FTIR spectra of hydrated type I collagen (hydrated in the same range as dermis samples, namely containing 65–70 % of water) and purified triglycerides are superimposed on this figure.

Absorption bands in fresh and stored and dermis samples were identified using FTIR data on peptides, protein [75–79] and biological tissues [80–85], peculiarly collagens [63, 80, 86–89] and dermis [17, 90, 91] and probable bands assignments are listed on Table 1.

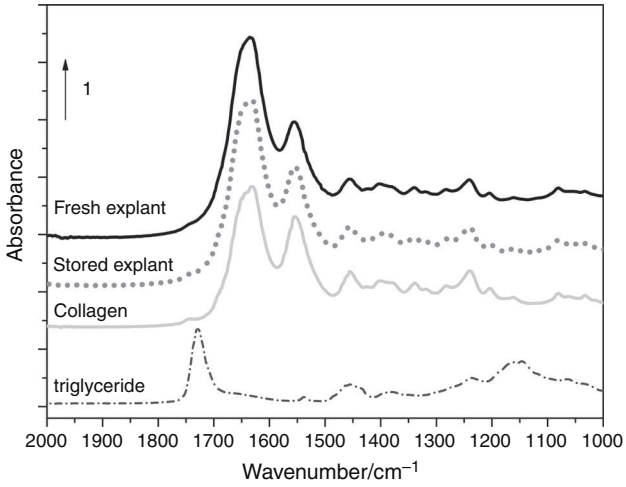

Fig. 7 Representative mean normalized FTIR spectra in the 2000–1000 cm^{-1} zone for a matched set of fresh and stored dermis, hydrated type I collagen and purified triglycerides

The classical absorption bands of proteins (amides I, II and III) are found on the spectra of fresh and stored derma, and their positions are very close to the absorption bands of pure type I collagen. In peculiar, collagen absorption features in the fingerprint region (the specific triplet of bands at 1204, 1238 and 1280 cm^{-1} [81, 92] as well as the specific band at 1338 cm^{-1}) [15, 81] are found in dermis samples, and the correlation coefficient between collagen and dermis spectra is more than 0.95 in this zone.

The very weak absorption in the 1740–1720 cm^{-1} zone, corresponding to the specific absorption of the carbonyl stretching of ester bond of phospholipids, unsaturated triglycerides and cholesterol esters [93, 94] confirms the clean-up of hypodermis in these dermis samples.

In order to enhance the resolution, the second derivative spectra in the amide I/amide II, which are sensitive to protein secondary structures, were displayed in Fig. 8.

The different minima detected in this zone were clearly identified as constant in dermis spectra and not considered as artefacts. The comparison of the second derivative spectra confirms the close correlation between collagen and fresh/stored dermis, with the main minima at of the amide I at 1694 cm^{-1} (anti-parallel β sheets), 1682 cm^{-1} (anti-parallel β sheets and β turns), 1667 cm^{-1} (turns, non H bonded loops), 1659 cm^{-1} (α helices), 1651 (random/helices), 1640–1636 cm^{-1} (intermolecular water), 1627 cm^{-1} (intramolecular β-sheets) and 1618 cm^{-1} (intermolecular β-sheets). According to previous studies on cardiovascular tissues [95], the spectral band at 1659 cm^{-1} attributed to α-helical structure is particularly representative of the exclusive α-helical structure of collagen [87].

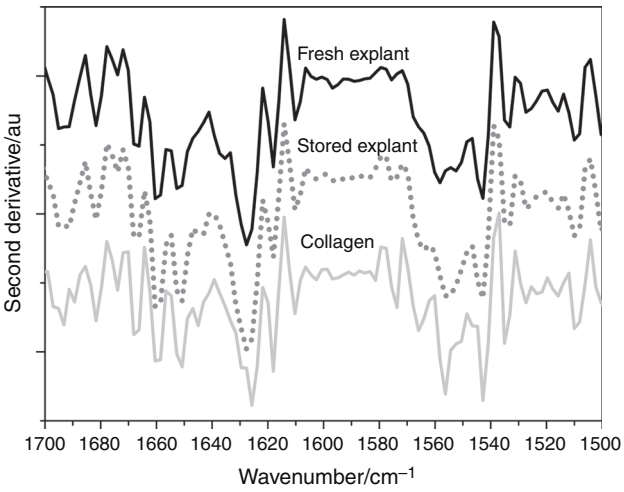

Fig. 8 Mean representative second derivative spectra of fresh and stored dermis and hydrated type I collagen

The main minima of the amide II, even if the assignation to peculiar secondary structures is less straightforward in the case of complex tissues [95], are located at 1555, 1543 and 1534 cm^{-1} in collagen and dermis explants. In a wide class of tissues, the vibration bands at around 1550 cm^{-1} are generally addressed to β-sheet conformations and the bands in the 1546–1540 cm^{-1} are attributed to helical conformations [81]; in pure freeze-dried collagen, a band at 1549 cm^{-1} is associated with triple helix structure cm^{-1} while a band at lower wavenumber (1530 cm^{-1}) is ascribed to disorder collagen [88]. Side-chain absorptions are well detected at 1510 cm^{-1} (Phe, Tyr) [88], 1527 cm^{-1}

Table 1 FTIR bands assignment of fresh and stored skin dermis

Band position/cm^{-1}	Assignment
1744	ν(C=O) triglycerides, cholesterol esters, phospholipids
1694–1630	ν(C=O) amide I, δ(O–H) water
1558–1542	ν(C–N), δ (N–H) amide II
1520, 1515, 1507	Side chains (tyrosine, phenylalanine)
1452	δ(CH2, CH3) mainly from proteins and lipids
1401–1393	ν_s(COO–) free amino acids, fatty acid
1338	CH_2 side-chain rotation (proline) specific band of collagen
1312	ν(C–N), and δ(N–H) amide III
1282	δ(CH3) specific of collagen
1239	Amide III, $\nu_{as}(PO_2^-)$ nucleic acid, phospholipids
1204	ν(C–OH) specific of collagen
1167–1156	ν_{as}(CO–O–C) esters de cholesterol, phospholipids
1086–1082	$\nu_s(PO_2^-)$nucleic acids, phospholipids, phosphorylated proteins
	ν(C–O) oligosaccharides, glycolipids
	ν(C–O) and ν(C–O–C) of the carbohydrate moieties in collagen
1032	ν_s(CO–OC) polysaccharides, collagen

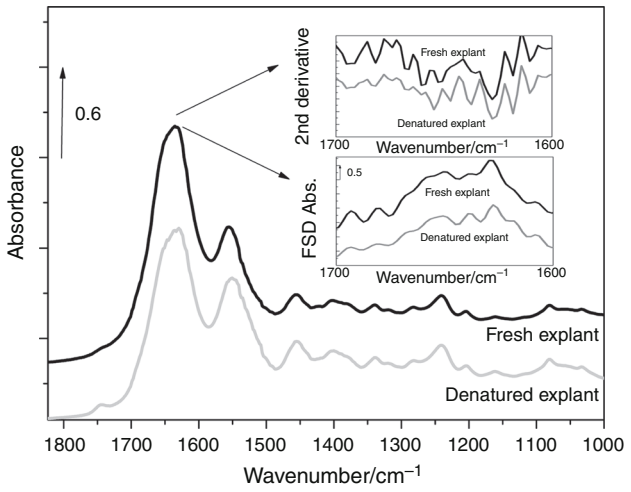

Fig. 9 Representative mean normalized FTIR spectra in the 1800–1000 cm^{-1} zone of fresh and heat-denatured dermis samples. Inset: Mean representative second derivative spectra and FSD of fresh and heat-denatured dermis samples in the amide I zone

(Lysine), 1576 cm^{-1} (Asp, Trp) and 1609 cm^{-1} (Gln) [75]. It is noteworthy that the position of the vibration bands in the global FTIR spectra and in the second derivative spectra in the 2100–950 cm^{-1} zone are identical in fresh and stored dermis, validating the conservation of the protein secondary structures with storage and thus validating this protocol.

To complete the research of biomarkers of collagen integrity, a selected set of biopsies was denatured by heating at 10 °C min^{-1} from 20 to 85 °C in hermetic pans according to previous DSC data. Global spectra of fresh and denatured samples in the amide I/II zone as well as the second derivative and FSD spectra in the amide I zone are reported in Fig. 9. The comparison between FTIR spectra of fresh and DSC-denatured derma lead to two main differences: the first one is the enhancement of the vibration band at 1740 cm^{-1}, attributed to the stretching vibration of carbonyl group of ester bonds. Such an enhancement has been already detected in gelatin (denatured collagen) [87, 88] but no hypothesis was proposed to explain it. We may assume that it comes from a chemical alteration of collagen in derma occurring during heating. The second important discrepancy is the shift of the amide II band toward low wavenumber in DSC-denatured derma. Such a behavior has been already reported in previous work on heat-denatured collagen films [88]. This shift toward low wavenumber of the amide II band can be explained by the depletion of the triple helical structure of collagen and the enhancement of disordered structures [88].

The comparison between the second derivative spectra or FSD spectra highlights the evolution of the proteins secondary structures with the DSC denaturation: the most important difference is the depletion of the band at 1659 cm^{-1}—previously addressed to α-helical structures [95]—and the occurrence of a new band at 1654 cm^{-1} that can be ascribed to destabilized helices or disordered structures. This evolution with denaturation has already been assumed in literature data for collagen [87, 88]. It confirms the assignment of the absorption band at 1659 cm^{-1} to the vibrational signature of the native triple helix of collagen. This absorption band can be considered as a good biomarker of collagen integrity in dermis, while the absorption band at 1654 cm^{-1} is ascribed to a marker of altered collagen. On the other hand, the second derivative or FSD of amide II region shows less difference between fresh and denatured skin sample compared to the amide I region.

Conclusions

Through the combined use of thermal and vibrational techniques, we can clearly find out that there is no significant influence of the storage effect of explants on the hydric organization, thermal characteristics of the denaturation endotherm and secondary structures of proteins in human skins. Moreover, this works evidences that DSC is well-suited technique to evaluate the hydric organization of biological tissue like human skin, giving accurate results with a high reproducibility. Combined with FTIR, the use of DSC allows the identification of reproducible and suitable biomarkers of the main protein in dermis, namely collagen, from the nanometric to the mesoscopic scale in biopsies 4 mm in diameter. The denaturation temperature of collagen $1/(1/T)_{mean}$, including the asymmetry of the endotherm, is a reliable biomarker of the intrinsic thermal stability of collagens in the skin, independent on the hydration of fresh skin. Moreover, the denaturation enthalpy can be considered as another suitable biomarker for the hydrogen bonds network of hydrated collagen in skin. Finally, the assignment of the different vibration bands of the amide I and II in human skin explants has been corroborated thanks to the comparison of fresh and DSC-denatured skin explants, allowing the quantification of the different secondary structures of proteins and side chains in dermis trough the decomposition the amide I and II peaks.

After the validation of this DSC/FTIR protocol, the perspectives will be focused on its application and the evolution of the evidenced biomarkers with enzymatic degradation of collagen in dermis, which will be biologically relevant. Finally, these protocols will be applied in the scheduled clinical study on young and aging biopsies (from 30 female 20–30 years old and from 30 female 60–70 years old) for further investigations on intrinsic and extrinsic aging of dermis.

References

1. Waller JM, Maibach HI. Age and skin structure and function, a quantitative approach (II): protein, glycosaminoglycan, water, and lipid content and structure. Skin Res Technol. 2006;12:145–54.
2. Kammeyer A, Luiten RM. Oxidation events and skin aging. Ageing Res Rev. 2015;21C:16–29.
3. Jung J-W, Cha S-H, Lee S-C, Chun I-K, Kim Y-P. Age-related changes of water content in the rat skin. J Dermatol Sci. 1997;14:12–9.
4. Carrino DA, Onnerfjord P, Sandy JD, Cs-Szabo G, Scott PG, Sorrell JM, Heinegård D, Caplan AI. Age-related changes in the proteoglycans of human skin. Specific cleavage of decorin to yield a major catabolic fragment in adult skin. J Biol Chem. 2003;278:17566–72.
5. Ngan CL, Basri M, Tripathy M, Karjiban RA, Abdul-Malek E. Skin intervention of fullerene-integrated nanoemulsion in structural and collagen regeneration against skin aging. Eur J Pharm Sci. 2015;70:22–8.
6. Krieg T, Aumailley M. The extracellular matrix of the dermis: flexible structures with dynamic functions. Exp Dermatol. 2011;20:689–95.
7. Song HK, Wehrli FW, Ma J. In vivo MR microscopy of the human skin. Magn Reson Med. 1997;37:185–91.
8. Tajima S, Nishikawa T, Hatano H. Distribution of macromolecular components in human dermal connective tissue. Public Health. 1982;273(1–2):115–20.
9. Cleary E. Skin. In: Comper W, editor. Extracellular matrix. Amsterdam: Harwood Academic Publishers; 1996. p. 77–109.
10. Verdier-Sévrain S, Bonté F. Skin hydration: a review on its molecular mechanisms. J Cosmet Dermatol. 2007;6:75–82.
11. Brincat M, Versi E, Moniz CF, Magos A, De Trafford J, Studd JWW. Skin collagen changes in postmenopausal women receiving different regimens of estrogen therapy. Obstet Gynecol. 1987;70:123–7.
12. Miyamae Y, Yamakawa Y, Kawabata M, Ozaki Y. A combined near-infrared diffuse reflectance spectroscopy and principal component analysis method of assessment for the degree of photoaging and physiological aging of human skin. Anal Sci. 2012;28:1159–64.
13. Attas EM, Sowa MG, Posthumus TB, Schattka BJ, Mantsch HH, Zhang SL. Near-IR spectroscopic imaging for skin hydration: the long and the short of it. Biopolymers. 2002;67:96–106.
14. Andanson J-M, Chan KLA, Kazarian SG. High-throughput spectroscopic imaging applied to permeation through the skin. Appl Spectrosc. 2009;63:512–7.
15. Canuto HC, Fishbein KW, Huang A, Doty SB, Herbert RA, Peckham J, Pleshko N, Spencer RG. Characterization of skin abnormalities in a mouse model of osteogenesis imperfecta using high resolution magnetic resonance imaging and Fourier transform infrared imaging spectroscopy. NMR Biomed. 2012;25:169–76.
16. Gniadecka M, Nielsen OF, Wessel S, Heidenheim M, Christensen DH, Wulf HC. Water and protein structure in photoaged and chronically aged Skin. J Invest Dermatol. 1998;111:1129–33.
17. Bonnier F, Ali SM, Knief P, Lambkin H, Flynn K, McDonagh V, Healy C, Lee TC, Lyng FM, Byrne HJ. Analysis of human skin tissue by Raman microspectroscopy: dealing with the background. Vib Spectrosc. 2012;61:124–32.
18. Fendel S, Schrader B. Investigation of skin and skin lesions by NIR-FT-Raman spectroscopy. Fresenius J Anal Chem. 1998;360: 609–13.
19. Zhang Q, Andrew Chan KL, Zhang G, Gillece T, Senak L, Moore DJ, Mendelsohn R, Flach CR. Raman microspectroscopic and dynamic vapor sorption characterization of hydration in collagen and dermal tissue. Biopolymers. 2011;95:607–15.
20. McGee MP, Morykwas M, Shelton J, Argenta L. Collagen unfolding accelerates water influx, determining hydration in the interstitial matrix. Biophys J. 2012;103:2157–66.
21. Wright AC, Bohning DE, Pecheny AP, Spicer KM. Magnetic resonance chemical shift microimaging of aging human skin in vivo: initial findings. Ski Res Technol. 1998;4:55–62.
22. Aktas N, Tülek Y, Gökalp HY. Determination of freezable water content of beef semimembranous muscle DSC study. J Therm Anal. 1997;48:259–66.
23. Panagopoulou A, Kyritsis A, Aravantinou AM, Nanopoulos D, i Serra RS, GómezRibelles JL, Shinyashiki N, Pissis P. Glass transition and dynamics in lysozyme–water mixtures over wide ranges of composition. Food Biophys. 2011;6:199–209.
24. Samouillan V, Tintar D, Lacabanne C. Hydrated elastin. Dynamics of water and protein followed by dielectric spectroscopies. Chem Phys. 2011;385:19–26.
25. Kerch G, Zicans J, Merijs RM, Stunda-Ramava A, Jakobson E. The use of thermal analysis in assessing the effect of bound water content and substrate rigidity on prevention of platelet adhesion. J Therm Anal Calorim. 2015;120:533–9.
26. Miles CA, Burjanadze TV, Bailey AJ. The kinetics of the thermal denaturation of collagen in unrestrained rat tail tendon determined by differential scanning calorimetry. J Mol Biol. 1995;245:437–46.
27. Miles CA, Ghelashvili M. Polymer-in-a-box mechanism for the thermal stabilization of collagen molecules in fibers. Biophys J. 1999;76:3243–52.
28. Lee J, Pereira C, Abdulla D, Naimark W, Crawford I. A multisample for collagenous denaturation biomaterials temperature tester. Mol Eng phys. 1995;17:115–21.
29. Samouillan V, Dandurand-Lods J, Lamure A, Maurel E, Lacabanne C, Gerosa G, Venturini A, Casarotto D, Gherardini L, Spina M. Thermal analysis characterization of aortic tissues for cardiac valve bioprostheses. J Biomed Mater Res. 1999;46:531–8.
30. Budrugeac P. Phase transitions of a parchment manufactured from deer leather. J Therm Anal Calorim. 2015;120:103–12.
31. Nöt LG, Naumov I, Vámhidy L, Lőrinczy D, Wiegand N. Comparison of thermal characteristics of degenerated and inflamed human collagen structures with differential scanning calorimetry. J Therm Anal Calorim. 2012;113:273–9.
32. Torres K, Trębacz H, Bącik-Donica M, Atras A, Torres A, Plewa Z. Does thermodynamic stability of peritoneal collagen change during laparoscopic cholecystectomies? A differential scanning calorimetry (DSC) study. Surg Endosc. 2014;28:2623–6.
33. Burton B, Gaspar A, Josey D, Tupy J, Grynpas MD, Willett TL. Bone embrittlement and collagen modifications due to high-dose gamma-irradiation sterilization. Bone. 2014;61:71–81.
34. Flandin F, Buffevant C, Herbage D. A differential scanning calorimetry analysis of the age-related changes in the thermal stability of rat skin collagen. Biochim Biophys Acta Protein Struct Mol Enzymol. 1984;791:205–11.
35. Le Lous M, Flandin F, Herbage D, Allain JC. Influence of collagen denaturation on the chemorheological properties of skin, assessed by differential scanning calorimetry and hydrothermal isometric tension measurement. Biochim Biophys Acta Gen Subj. 1982;717:295–300.
36. Miles CA, Avery NC. Thermal stabilization of collagen in skin and decalcified bone. Phys Biol. 2011;8:026002.
37. Sun WQ, Leung P. Calorimetric study of extracellular tissue matrix degradation and instability after gamma irradiation. Acta Biomater. 2008;4:817–26.
38. Melling M, Pfeiler W, Karimian-Teherani D, Schnallinger M, Sobal G, Zangerle C, Menzel EJ. Differential scanning calorimetry, biochemical, and biomechanical analysis of human skin from individuals with diabetes mellitus. Anat Rec. 2000;259: 327–33.

39. Wiegand N, Naumov I, Nőt LG, Vámhidy L, Lőrinczy D. Differential scanning calorimetric examination of pathologic scar tissues of human skin. J Therm Anal Calorim. 2012;111:1897–902.
40. Fathima NN, Kumar MP, Rao JR, Nair BU. A DSC investigation on the changes in pore structure of skin during leather processing. Thermochim Acta. 2010;501:98–102.
41. Brun M, Lallemand A, Quinson J-F, Eyraud C. A new method for the simultaneous determination of the size and shape of pores: the thermoporometry. Thermochim Acta. 1977;21:59–88.
42. Landry MR. Thermoporometry by differential scanning calorimetry: experimental considerations and applications. Thermochim Acta. 2005;433:27–50.
43. Ishikiriyama K, Todoki M, Kobayashi T, Tanzawa H. Pore size distribution measurements of poly(methyl methacrylate) hydrogel membranes for artificial kidneys using differential scanning calorimetry. J Colloid Interface Sci. 1995;173:419–28.
44. Majda D, Makowski W, Mańko M. Pore size distribution of micelle-templated silicas studied by thermoporosimetry using water and *n*-heptane. J Therm Anal Calorim. 2012;109:663–9.
45. Ishikiriyama K, Todoki M, Motomura K. Pore size distribution (PSD) measurements of silica gels by means of differential scanning calorimetry. J Colloid Interface Sci. 1995;171:92–102.
46. Fashandi H, Karimi M. Characterization of porosity of polystyrene fibers electrospun at humid atmosphere. Thermochim Acta. 2012;547:38–46.
47. Hay JN, Laity PR. Observations of water migration during thermoporometry studies of cellulose films. Polymer (Guildf). 2000;41:6171–80.
48. Heys KR, Friedrich MG, Truscott RJW. Free and bound water in normal and cataractous human lenses. Invest Ophthalmol Vis Sci. 2008;49:1991–7.
49. Gniadecka M, Nielsen OF, Christensen DH, Wulf HC. Structure of water, proteins, and lipids in intact human skin, hair, and nail. J Invest Dermatol. 1998;110:393–8.
50. Perry A, Stypa MP, Tenn BK, Kumashiro KK. On Elastin C NMR reveals effects of temperature and hydration. Biophys J. 2002;82:1086–95.
51. Panagopoulou A, Kyritsis A, Vodina M, Pissis P. Dynamics of uncrystallized water and protein in hydrated elastin studied by thermal and dielectric techniques. Biochim Biophys Acta. 2013;1834:977–88.
52. Leveque JL, Garson JC, Boudouris G. Water in keratin: study of the depolarization thermal current peak II. Biopolymers. 1977;16:1725–33.
53. Kaatze U. The dielectric properties of water in its different states of interaction. J Solution Chem. 1997;26:1049–112.
54. Melacini G, Bonvin AM, Goodman M, Boelens R, Kaptein R. Hydration dynamics of the collagen triple helix by NMR. J Mol Biol. 2000;300:1041–9.
55. Hatakeyama H, Hatakeyama T. Interaction between water and hydrophilic polymers. Thermochim Acta. 1998;308:3–22.
56. Einhorn-Stoll U, Hatakeyama H, Hatakeyama T. Influence of pectin modification on water binding properties. Food Hydrocoll. 2012;27:494–502.
57. Samouillan V, Delaunay F, Dandurand J, Merbahi N, Gardou JP, Yousfi M, Gandaglia A, Spina M, Lacabanne C. The use of thermal Techniques for the characterization and selection of natural biomaterials. J Funct Biomater. 2011;2:230–48.
58. Nandi N, Bhattacharyya K, Bagchi B. Dielectric relaxation and solvation dynamics of water in complex chemical and biological systems. Chem Rev. 2000;100:2013–46.
59. Gevorkian SG, Allahverdyan AE, Gevorgyan DS, Simonian AL, Hu CK. Stabilization and anomalous hydration of collagen fibril under heating. PLoS ONE. 2013;8(11):e78526.
60. Bella J, Brodsky B, Berman HM. Hydration structure of a collagen peptide. Structure. 1995;3:893–906.
61. Pouliot R, Germain L, Auger F, Tremblay N, Juhasz J. Physical characterization of the stratum corneum of an in vitro human skin equivalent produced by tissue engineering and its comparison with normal human skin by ATR-FTIR spectroscopy and thermal analysis (DSC). Biochim Biophys Acta. 1999;1439:341–52.
62. Babita K, Kumar V, Rana V, Jain S, Tiwary AK. Thermotropic and spectroscopic behavior of skin: relationship with percutaneous permeation enhancement. Curr Drug Deliv. 2006;3:95–113.
63. Sionkowska A, Skopinska-Wisniewska J, Gawron M, Kozlowska J, Planecka A. Chemical and thermal cross-linking of collagen and elastin hydrolysates. Int J Biol Macromol. 2010;47:570–7.
64. Sionkowska A, Kamińska A. Thermal helix-coil transition in UV irradiated collagen from rat tail tendon. Int J Biol Macromol. 1999;24:337–40.
65. Privalov PL, Tiktopulo EI, Tischenko VM. Stability and mobility of the collagen structure. J Mol Biol. 1979;127:203–16.
66. Balian G, Bowes JH. The structure and properties of collagen. In: Ward AG, Courts A, editors. The Science and Technology of Gelatin. London: Academic Press Inc.; 1977. p. 1–27.
67. Flory PJ, Garrett RR. Phase transitions in collagen and gelatin systems 1. J Am Chem Soc. 1958;80:4836–45.
68. Bruylants G, Wouters J, Michaux C. Differential scanning calorimetry in life science: thermodynamics, stability, molecular recognition and application in drug design. Curr Med Chem. 2005;12:2011–20.
69. Urschitz J, Iobst S, Urban Z, Granda C, Souza KA, Lupp C, Schilling K, Scott I, Csiszar K, Boyd CD. A serial analysis of gene expression in sun-damaged human skin. J Invest Dermatol. 2002;119(1):3–13.
70. Takada S, Naito S, Sonoda J, Miyauchi Y. Noninvasive in vivo measurement of natural moisturizing factor content in stratum corneum of human skin by attenuated total reflection infrared spectroscopy. Appl Spectrosc. 2012;66:26–32.
71. Brancaleon L, Bamberg MP, Sakamaki T, Kollias N. Attenuated total reflection Fourier transform infrared spectroscopy as a possible method to investigate biophysical parameters of stratum corneum in vivo. J Invest Dermatol. 2001;116:380–6.
72. Zhang L, Aksan A. Fourier transform infrared analysis of the thermal modification of human cornea tissue during conductive keratoplasty. Appl Spectrosc. 2010;64:23–9.
73. Yu G, Zhang G, Flach CR, Mendelsohn R. Vibrational spectroscopy and microscopic imaging: novel approaches for comparing barrier physical properties in native and human skin equivalents. J Biomed Opt. 2013;18:061207.
74. Lucassen GW, Van Veen GN, Jansen JA. Band analysis of hydrated human skin stratum corneum attenuated total reflectance fourier transform infrared spectra in vivo. J Biomed Opt. 1998;3:267–80.
75. Barth A. The infrared absorption of amino acid side chains. Prog Biophys Mol Biol. 2000;74:141–73.
76. Barth A. Infrared spectroscopy of proteins. Biochim Biophys Acta. 2007;1767:1073–101.
77. Popescu MC, Vasile C, Craciunescu O. Structural analysis of some soluble elastins by means of FT-IR and 2D IR correlation spectroscopy. Biopolymers. 2010;93:1072–84.
78. Kong J, Yu S. Fourier transform infrared spectroscopic analysis of protein secondary structures protein FTIR data analysis and band assignment. Acta Biochem Biophys Sin. 2007;39:549–59.
79. Venyaminov S, Kalnin NN. Quantitative IR spectrophotometry of peptide compounds in water (H_2O) solutions. I. Spectral parameters of amino acid residue absorption bands. Biopolymers. 1990;30:1243–57.
80. Pluot M, Baehrel B, Manfait M, Rubin S, Bonnier F, Sandt C, Vente L. Analysis of structural changes in normal and aneurismal human aortic tissues using FTIR microscopy. Biopolymers. 2007;89:160–9.

81. Staniszewska E, Malek K, Baranska M. Rapid approach to analyze biochemical variation in rat organs by ATR FTIR spectroscopy. Spectrochim Acta A Mol Biomol Spectrosc. 2014;118: 981–6.
82. Cheheltani R, Rosano JM, Wang B, Sabri AK, Pleshko N, Kiani MF. Fourier transform infrared spectroscopic imaging of cardiac tissue to detect collagen deposition after myocardial infarction of cardiac tissue to detect collagen deposition. J Biomed Opt. 2012;17(5):056014.
83. Camacho NP, West P, Torzilli PA, Mendelsohn R. FTIR microscopic imaging of collagen and proteoglycan in bovine cartilage. Biopolymers. 2001;62:1–8.
84. Liu KZ, Dixon IM, Mantsch HH. Distribution of collagen deposition in cardiomyopathic hamster hearts determined by infrared microscopy. Cardiovasc Pathol. 1999;8:41–7.
85. Zohdi V, Wood BR, Pearson JT, Bambery KR, Black MJ. Evidence of altered biochemical composition in the hearts of adult intrauterine growth-restricted rats. Eur J Nutr. 2013;52:749–58.
86. Belbachir K, Noreen R, Gouspillou G, Petibois C. Collagen types analysis and differentiation by FTIR spectroscopy. Anal Bioanal Chem. 2009;395:829–37.
87. Payne KJ, Veis A. Fourier transform IR spectroscopy of collagen and gelatin solutions: deconvolution of the amide I band for conformational studies. Biopolymers. 1988;27:1749–60.
88. Rabotyagova OS, Cebe P, Kaplan DL. Collagen structural hierarchy and susceptibility to degradation by ultraviolet radiation. Mater Sci Eng C Mater Biol Appl. 2008;28:1420–9.
89. Petibois C, Gouspillou G, Wehbe K, Delage J-P, Déléris G. Analysis of type I and IV collagens by FT-IR spectroscopy and imaging for a molecular investigation of skeletal muscle connective tissue. Anal Bioanal Chem. 2006;386:1961–6.
90. Tfayli A, Piot O, Durlach A, Bernard P, Manfait M. Discriminating nevus and melanoma on paraffin-embedded skin biopsies using FTIR microspectroscopy. Biochim Biophys Acta. 2005; 1724:262–9.
91. Tetteh J, Mader KT, Andanson JM, McAuley WJ, Lane ME, Hadgraft J, Kazarian SG, Mitchell JC. Local examination of skin diffusion using FTIR spectroscopic imaging and multivariate target factor analysis. Anal Chim Acta. 2009;642:246–56.
92. Wang Q, Sanad W, Miller LM, Voigt A, Klingel K, Kandolf R, Stangl K, Baumann G. Infrared imaging of compositional changes in inflammatory cardiomyopathy. Vib Spectrosc. 2005;38: 217–22.
93. Krilov D, Balarin M, Kosović M, Gamulin O, Brnjas-Kraljević J. FT-IR spectroscopy of lipoproteins—a comparative study. Spectrochim Acta A Mol Biomol Spectrosc. 2009;73:701–6.
94. Nara M, Okazaki M, Kagi H. Infrared study of human serum very-low-density and low-density lipoproteins. Implication of esterified lipid C=O stretching bands for characterizing lipoproteins. Chem Phys Lipids. 2002;117:1–6.
95. Bonnier F, Rubin S, Debelle L, Ventéo L, Pluot M, Baehrel B, Manfait M, Sockalingum GD. FTIR protein secondary structure analysis of human ascending aortic tissues. J Biophotonics. 2008;1:204–14.